JOURNAL OF CHEMICAL & ENGINEERING DATA

ARTICLE

pubs.acs.org/jced

Liquid−Liquid Phase Behavior of Solutions of 1-Hexyl-3-methylimidazolium Bis((trifluoromethyl)sulfonyl)amide (C_6mimNTf_2) in *n*-Alkyl Alcohols

Vlad R. Vale,[†] Bernd Rathke,[*,†] Stefan Will,[†] and Wolffram Schröer[‡]

[†]Technische Thermodynamik, Universität Bremen, Badgasteiner Str. 1, 28359 Bremen, Germany

[‡]Institut für Anorganische und Physikalische Chemie, Fachbereich 2, Universität Bremen, Leobener Str. NWII, 28359 Bremen, Germany

ABSTRACT: Liquid−liquid phase diagrams of binary mixtures of the ionic liquid 1-hexyl-3-methylimidazolium bis((trifluoromethyl)sulfonyl)amide (C_6mimNTf_2) with *n*-alkyl alcohols (hexan-1-ol, heptan-1-ol, octan-1-ol, nonan-1-ol, decan-1-ol, undecan-1-ol, dodecan-1-ol, and tetradecan-1-ol) are reported. By application of the cloud-point method on a set of samples, phase diagrams were obtained at atmospheric pressure over the temperature range (280 to 423) K. The investigated systems show partial miscibility with an upper critical solution temperature (UCST) between (306 and 401) K. With increasing chain length of the alcohol, the UCST shifts toward higher temperatures and slightly higher concentrations. Ising criticality was assumed in the numerical analysis of the phase diagrams. The analysis yielded the UCST, the corresponding critical composition, and the width and diameter parameters that characterize the shape of the phase diagrams. The temperature dependence of the diameter of the phase diagram, which determines the asymmetry of the phase diagram, is not linear as presumed by the rectilinear diameter rule of Cailletet-Mathias. Instead, as requested by the theory of complete scaling, it also depends on nonlinear, nonanalytical contributions that are the leading terms when the critical solution point is approached. The shapes of the phase diagrams of the investigated solutions are very similar when the data are represented in terms of corresponding-states variables.

INTRODUCTION

In this work, we continued our systematic investigation of solutions of ionic liquids (ILs) of the type 1-alkyl-3-methylimidazolium bis((trifluoromethyl)sulfonyl)amide ($C_x$mimNTf_2) in *n*-alkyl alkohols[1,2] by considering solutions of 1-hexyl-3-methylimidazolium bis((trifluoromethyl)sulfonyl)amide (C_6mimNTf_2). Former studies concerned the ILs $C_x$mimNTf_2 with $x = 8, 10, 12$.[1,2]

The data are intended to provide the basis for chemical engineering work[3−5] and the development of equations of state for solutions of ILs with relevance (e.g., for extractions[6−9] and two-phase reactions[10]). We have systematically studied the influence of the chain length of the alcohol and the length of the side chains of the IL on the thermodynamic properties of the IL solutions. Of particular interest is the behavior when the salt and the alcohol become highly hydrophobic.

A reliable representation of thermodynamic data (e.g., phase diagrams) with a minimum of parameters is useful and can be achieved on the basis of adequate models.[3,4] Theoretical models refining the van der Waals equation[3,4,11] or the theory of regular solutions[3,4,12] or using the quasi-chemical approximation[3,5,13] have proved to be useful tools in chemical engineering. However, all of these approaches are mean-field theories that do not take into account fluctuations, which become important in the vicinity of critical points (CPs), including the upper critical solution point (UCSP) of liquid−liquid phase transitions as considered in this paper. Mean-field models fail fundamentally, for example, when describing phase diagrams in the region near such critical points. By now it is appreciated that both the liquid−gas and liquid−liquid phase transitions of nonionic systems show the same universal critical properties as the 3D Ising model,[4,14−16] which is a simple lattice model. The temperature dependence of the difference between the compositions in the coexisting phases is universally determined by the power law $|T - T_c|^{\beta}$, which depends on the separation of the transition temperatures T from the critical temperature T_c of the phase transition considered. The exponent β takes up the universal value $\beta = 0.326$,[4,14−16] while all mean-field theories yield a β value of 0.5, in contrast to the experiments. The Ising model is the simplest model that allows for a two-phase equilibrium. It is simple enough to allow simulations in the critical region, which require a large number of particles.[17] Clearly, such a simple model is not apt to take into account the specific molecular properties, as the elaborated mean-field models do.[3−5,11−13] Thus, approximate methods that fill this gap have been proposed,[18−20] they are urgently required for application and are a field of current research.[21]

Ising criticality is generally expected when the phase transition is driven by short-range r^{-n} interactions, where $n \geq 4.97$.[22] Thus, mean-field criticality is expected for phase transitions in ionic systems because the long-range Coulomb interactions vary with r^{-1}.[23−26] According to experiments[27−33] and simulations that apply finite-size scaling techniques,[34−36] it is now almost certain that the liquid−gas phase transition of salts and the liquid−liquid phase transition in ionic solutions also show Ising behavior because the correlations become short-ranged as a result of

Special Issue: John M. Prausnitz Festschrift

Received: October 29, 2010
Accepted: March 8, 2011
Published: March 24, 2011

cooperative shielding of the ions,[37−39] as already described by the Debye−Hückel theory. Experiments on ionic solutions yielding mean-field critical behavior[40,41] could not be reproduced.[27] Quite likely, experimental deficiencies are the reason when other than Ising criticality is found.[33] For reviews of the story of criticality in Coulombic systems, see refs 26, 42, and 43.

However, there is a marked difference between the phase diagram of the Ising model and those for real systems. While the Ising model is symmetric, the phase diagrams of the liquid−gas and liquid−liquid phase transitions are in general asymmetric. The asymmetry of the phase diagrams of ionic systems is known to be particularly large,[44] but systematic investigations are missing. The asymmetry implies that the average composition of the two phases, called the diameter, is not constant but varies with temperature. This is already included in the van der Waals equation.[4,11] However, the van der Waals equation and all mean-field theories predict that the diameter of the phase diagram should vary linearly with the temperature[4,11,22] near the critical point. This behavior, termed the rectilinear diameter rule of Cailletet-Mathias,[45] appeared to be well-established for almost a century and was used as a tool for estimating critical data.[4] However, the temperature dependence of the diameters of coexistence curves of liquid−gas and liquid−liquid transitions in binary mixtures is not linear and even becomes nonanalytical as a CP is approached. According to the recently developed theory of "complete scaling", the temperature dependence of the diameter can be described by a power series in $|T - T_c|$ involving a linear term and nonanalytical terms[46−49] with exponents of $1 - \alpha$ and 2β, respectively. Thus, a Taylor expansion in powers of $|T - T_c|$ with natural numbers as exponents is not appropriate. The term determined by the exponent 2β is in general the leading term.[50−52] We recall that $\alpha = 0.11$ is the critical exponent determining the divergence of the specific heat.[4,14−16,46−49] An overview of the crossover from Ising to mean-field criticality and complete scaling for the liquid−gas transition of one-component systems and the liquid−liquid transition in binary mixtures is provided in a recent review by Behnejad et al.[53]

Quite a few phase diagrams for liquid−liquid phase transitions of solutions of ILs have been reported lately.[1,2,54−76] Nevertheless, systematic studies are still required for assessing the relations between the phase diagrams and the chemical structures of the components by empirical analysis and theoretical methods. Investigations of mixtures with alcohols are informative because varying the chain length of the alcohol changes not only the relative size of the components of the solution but also the dielectric permittivity and the ratio of the polar OH group to the nonpolar tail. In principle, such investigations can cover the range from highly polar to nonpolar solvents[54,56,63] (e.g., from water[54−56] to hydrocarbons[63−66]). Phase diagrams of solutions of ILs with BF_4^- or PF_6^- as the anion have been reported in some detail,[54−62] as have those for solutions of ILs with halide anions.[63−66] ILs with the anion bis((trifluoromethyl)sulfonyl)amide (NTf_2^-) are of particular interest because this anion is rather hydrophobic, making the ILs soluble in nonpolar solvents.[67−70] ILs with the NTf_2^- anion are more stable against hydrolysis than ILs with either BF_4^- or PF_6^-.[77] Work on solutions of ILs with the NTf_2^- anion has involved solutions in aprotic solvents[67−70] and alcohol solutions.[1,2,60−62,71−76] Here we extend the investigations of the rather polar *n*-alkyl alcohols with small chain lengths (n = 2 to 6) to solutions of less polar alcohols with longer chain lengths (n = 10 to 14). Phase diagrams of solutions of ILs with long-chain alcohols that have an upper critical solution temperature (UCST) near ambient conditions can be expected for ILs that are rather hydrophobic, which in addition to the hydrophobic NTf_2^- anion requires a cation with a long side chain. However, varying the length of the side chain of the methylimidazolium cations causes not only changes in the hydrophobicity of the ILs but also structural changes. With increasing length of the side chain, the methylimidazolium salts $C_x$mim show an increasing tendency for microscopic segregation of the salts into ionic and hydrophobic regions.[78,79] For longer side chains ($x > 10$), liquid-crystalline domains are formed for salts with the anions Cl^-, Br^-, BF_4^-, and PF_6^-. This complication can be avoided by considering ILs with the NTf_2^- anion,[80] which is nonspherical and has different conformers.[81] We report here eight phase diagrams for mixtures of 1-hexyl-3-methylimidazolium bis((trifluoromethyl)sulfonyl)-amide (C_6mimNTf_2) (Figure 1) with *n*-alkyl alcohols (n = 6, 7, 8, 9, 10, 11, 12, 14), supplementing our previous report on solutions of C_8mimNTf_2,[1] C_{10}mimNTf_2,[1] and C_{12}mimNTf_2.[2] We have included data for solutions in butan-1-ol[75] and pentan-1-ol[75] in the analysis and also made comparisons with data for solutions in hexan-1-ol[62,73,75,76] and octan-1-ol[75,76] reported by others. A numerical data analysis was carried out in order to get the parameters characterizing the phase diagrams and allow for a quantitative assessment of the influence of the chain length of the alcohol on the location and shape of the phase diagram. For the data analysis, Ising criticality was assumed, and a linear term or a nonanalytical term with an exponent of 2β was taken into account for modeling of the diameter. A subsequent corresponding-states analysis with the reduced variables $|T - T_c|/T_c$ and $(x - x_c)/x_c$, where x is the mole fraction of the IL and x_c is the mole fraction at the UCST obtained by the preceding analysis, demonstrated that the phase diagrams in the scaled variables are almost the same.

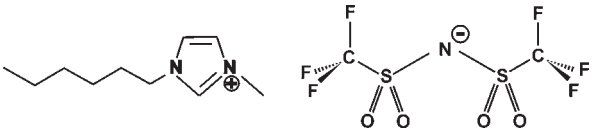

Figure 1. Structure of the ionic liquid 1-hexyl-3-methylimidazolium bis((trifluoromethyl)sulfonyl) amide, abbreviated as C_6mimNTf_2.

EXPERIMENTAL SECTION

Materials. The *n*-alkyl alcohols hexan-1-ol [$C_6H_{14}O$, CAS no. 111-27-3, mass-fraction purity $w \geq 0.98$, dielectric permittivity $\varepsilon(T = 298.15\ K) = 12.17$[82]], heptan-1-ol [$C_7H_{16}O$, CAS no. 111-70-6, $w \geq 0.99$, $\varepsilon(T = 298.15\ K) = 10.78$[82]], octan-1-ol [$C_8H_{18}O$, CAS no. 111-87-5, $w \geq 0.99$, $\varepsilon(T = 298.15\ K) = 9.60$[82]], nonan-1-ol [$C_9H_{20}O$, CAS no. 143-08-8, $w \geq 0.98$, $\varepsilon(T = 298.15\ K) = 8.18$[82]], decan-1-ol [$C_{10}H_{22}O$, CAS no. 112-30-1, $w \geq 0.99$, $\varepsilon(T = 298.15\ K) = 7.66$[82]], undecan-1-ol [$C_{11}H_{24}O$, CAS no. 112-42-5, $w \geq 0.98$, $\varepsilon(T = 298.15\ K) = 6.74$[82]], dodecan-1-ol [$C_{12}H_{26}O$, CAS no. 112-53-8, $w \geq 0.99$, $\varepsilon(T = 298.15\ K) = 6.53$[82]], and tetradecan-1-ol [$C_{14}H_{30}O$, CAS no. 112-72-1, $w \geq 0.98$, $\varepsilon(T = 298.15\ K) = 5.19$[82]] were purchased from Merck (Darmstadt, Germany) with a maximum of available purity and were used without further purification. The IL C_6mimNTf_2 ($C_{12}H_{19}F_6N_3O_4S_2$, CAS no. 382150-50-7, $w > 0.99$, $H_2O < 100$ ppm) was purchased from IoLiTec (Ionic Liquids Technologies GmbH, Heilbronn, Germany) and degassed and dried before sample preparation. In order to remove the water and any volatiles, the IL C_6mimNTf_2 was added to a 100 mL round-bottom flask (Schott Duran glass)

Table 1. Data Set for the Liquid−Liquid Phase Diagrams of C_6mimNTf$_2$ + *n*-Alkyl Alcohol (C_nOH) Mixtures: Mass Fractions (w), Mole Fractions (x_{IL}), Cloud-Point Temperatures (T_{cloud}), and the Repeatabilities of the Determination of T_{cloud} (δT)[a]

w	x_{IL}	T_{cloud}/K	δT/K
	C_6mimNTf$_2$ + Hexan-1-ol		
0.078	0.019	294.28	0.05
0.119	0.030	299.48	0.05
0.178	0.047	303.19	0.05
0.218	0.060	304.57	0.05
0.273	0.079	305.49	0.05
0.327	0.100	305.92	0.05
0.432	0.148	306.05	0.05
0.521	0.199	305.69	0.05
0.591	0.248	304.81	0.05
0.651	0.299	302.73	0.05
0.695	0.342	300.62	0.05
0.745	0.400	296.65	0.05
0.780	0.447	292.71	0.05
	C_6mimNTf$_2$ + Heptan-1-ol		
0.070	0.019	306.42	0.05
0.112	0.032	312.44	0.06
0.127	0.036	315.13	0.08
0.160	0.047	316.20	0.05
0.237	0.075	318.81	0.06
0.299	0.100	319.85	0.07
0.402	0.149	320.30	0.05
0.487	0.198	320.14	0.07
0.564	0.251	319.33	0.05
0.615	0.293	317.98	0.06
0.672	0.348	315.63	0.05
0.722	0.403	312.15	0.06
0.757	0.448	309.00	0.11
0.795	0.501	304.33	0.18
	C_6mimNTf$_2$ + Octan-1-ol		
0.059	0.018	321.15	0.05
0.096	0.030	325.06	0.05
0.121	0.039	327.90	0.06
0.154	0.050	330.51	0.05
0.218	0.075	332.36	0.11
0.277	0.100	333.23	0.05
0.375	0.149	333.52	0.06
0.462	0.200	333.42	0.05
0.534	0.250	332.73	0.07
0.594	0.299	331.26	0.05
0.644	0.345	329.34	0.06
0.692	0.396	326.19	0.08
0.729	0.440	323.35	0.05
	C_6mimNTf$_2$ + Nonan-1-ol		
0.093	0.032	334.69	0.05
0.141	0.050	339.47	0.05
0.211	0.079	340.94	0.05
0.256	0.100	341.95	0.05
0.310	0.126	343.04	0.05
0.351	0.149	344.06	0.05
0.435	0.199	344.26	0.06
0.510	0.251	344.07	0.06
0.567	0.297	342.49	0.05
0.624	0.349	340.59	0.08
0.672	0.397	338.06	0.06
0.719	0.452	333.87	0.05
	C_6mimNTf$_2$ + Decan-1-ol		
0.053	0.020	340.98	0.05
0.081	0.030	348.81	0.05
0.105	0.040	349.99	0.05
0.128	0.050	352.32	0.05
0.190	0.077	354.35	0.07
0.239	0.100	355.71	0.05
0.273	0.117	355.63	0.06
0.329	0.148	356.34	0.05
0.416	0.201	356.15	0.06
0.483	0.248	355.77	0.09
0.545	0.297	354.63	0.05
0.608	0.354	353.13	0.05
0.650	0.397	350.82	0.05
0.702	0.455	348.05	0.05
	C_6mimNTf$_2$ + Undecan-1-ol		
0.074	0.030	350.39	0.06
0.120	0.050	356.05	0.05
0.224	0.100	363.21	0.05
0.313	0.149	364.09	0.05
0.393	0.200	364.22	0.05
0.462	0.249	364.18	0.05
0.523	0.297	364.10	0.05
0.587	0.354	362.65	0.07
0.634	0.400	360.67	0.05
0.685	0.456	358.28	0.05
	C_6mimNTf$_2$ + Dodecan-1-ol		
0.059	0.025	364.39	0.05
0.068	0.030	365.18	0.05
0.108	0.048	371.31	0.05
0.141	0.064	373.80	0.05
0.187	0.087	375.38	0.05
0.229	0.110	376.19	0.05
0.308	0.156	376.69	0.05
0.393	0.213	376.72	0.05
0.500	0.294	376.08	0.05
0.531	0.321	375.24	0.05
0.592	0.377	373.92	0.05
0.629	0.414	371.88	0.05
0.678	0.467	368.85	0.05
	C_6mimNTf$_2$ + Tetradecan-1-ol		
0.099	0.050	394.02	0.10
0.191	0.102	399.56	0.06
0.267	0.149	401.25	0.05
0.339	0.197	401.06	0.05

dx.doi.org/10.1021/je1011357 |*J. Chem. Eng. Data* 2011, 56, 1330–1340

Table 1. Continued

0.411	0.250	401.35	0.05
0.471	0.299	400.18	0.06
0.525	0.346	398.89	0.05
0.571	0.389	396.75	0.05
0.636	0.455	394.55	0.05
0.676	0.500	390.95	0.05

[a] The expanded uncertainty ($k = 2$) of T_{cloud} was $\Delta T = \pm 0.75$ K. The uncertainty in the mole fraction due to the accuracy of the weight measurement and the sample size was $\Delta x_{IL} = \pm 10^{-3}$.

under an inert argon atmosphere inside a glovebag (AtmosBag, Sigma-Aldrich) and dried under continuous stirring at a temperature of 318 K for about 12 h under a vacuum of $2 \cdot 10^{-5}$ bar. The drying process was frequently monitored by weighing the sample. We checked the mass loss of a sample containing typically 40 g of IL after the process of drying and found that the detectable loss of mass was less than 10^{-3} g within a period of 2 h.

Sample Preparation. The phase diagrams were determined using the synthetic method. Mixtures of IL and alcohol with different compositions were prepared in culture tubes (Schott Duran glass) with heat-resistant screw caps made of PBT with a PTFE-coated silicon seal under a protective gas atmosphere (argon), thus avoiding contact with air and humidity. A minimum of 10 samples with mole fractions between 0.02 and 0.45 were prepared for each binary mixture by weighing each component directly into the sample tube; the typical size of a sample was 2 g. The composition was determined gravimetrically with an accuracy of 10^{-3} g, resulting in an overall uncertainty in the mole fraction of $\Delta x_{IL} = \pm 10^{-3}$.

Cloud-Point Detection. The transition temperatures defining the liquid−liquid phase diagrams of the IL + alcohol binary mixtures were determined by the cloud-point method. For measurements in the lower temperature region [T = (280 to 340) K], a transparent water bath was used. The temperature stability was ± 0.02 K controlled by a thermostat (Haake DC 30, Thermo, Karlsruhe, Germany). In the higher temperature range [T = (340 to 430) K], measurements were carried out in a silicon oil bath with a temperature stability of better than ± 0.05 K (Proline RP845/PV15, Lauda, Lauda-Königshofen, Germany). In either case, the temperature was measured using a Pt-100 sensor connected to a high-precision resistance thermometer (Kelvimat 4323, Burster, Gernsbach, Germany) with an uncertainty of ± 0.05 K.

The cloud-point temperatures were determined visually as the onset of the phase transition. For this purpose, the temperature range and the temperature steps in the considered range were systematically reduced. At first, the prepared samples with known mole fraction were heated to about 5 K above the critical temperature for about 20 min and homogenized using either a vortex mixer or a magnetic stirrer. The temperature was then decreased in steps of typically (0.5 to 5) K until the two-phase region was reached. The temperature was increased again until the sample reached the one-phase region. These steps were repeated until the temperature interval in which the cloud-point temperature was observed within a time of up to 10 min reached 0.1 K near the critical point and (0.1 to 0.3) K near the edges of the phase diagrams. The cloud points and their repeatabilities (δT) were determined by repeating this procedure up to five times starting from the one-phase region at different initial temperatures followed by reducing the temperature in steps of 0.05 K at the top of the phase diagrams and in steps of (0.2 to 1) K at the edges. In Table 1, the cloud-point temperatures T_{cloud} and the values of δT are given. The influence of uncontrollable traces of impurities of the substances, which might have affected the results in a systematic way, was not taken into account. However, checks on different batches of the substances used in this study showed no significant variations. Together with the statistical error, this effect results in a slight scatter of the cloud-point temperatures, which can be estimated from the standard deviation of the fits from the experimental data (see Figure 3a,b). The combination of the accuracy of the T measurement and the standard deviation of the fits from the experimental data, which includes δT, results in an expanded uncertainty (coverage factor $k = 2$) of $\Delta T = 0.75$ K.

RESULTS AND DISCUSSION

Experimental Results. The data for the phase diagrams are listed in Table 1. We give the mass fractions, the IL mole fractions, and the cloud-point temperatures and their repeatabilities for the solutions of C_6mimNTf$_2$ in the *n*-alkyl alcohols hexan-1-ol (C_6OH), heptan-1-ol (C_7OH), octan-1-ol (C_8OH), nonan-1-ol (C_9OH), decan-1-ol (C_{10}OH), undecan-1-ol (C_{11}OH), dodecan-1-ol (C_{12}OH), and tetradecan-1-ol (C_{14}OH).

The phase diagrams are shown in Figure 2a−c. The composition variable is x, the mole fraction of the IL. Figure 2a provides an overview of all eight phase diagrams of the mixtures of C_6mimNTf$_2$ determined in this work. Figure 2b,c gives a closer look at the phase diagrams, with those for the alcohols C_6OH, C_7OH, C_8OH, and C_9OH shown in Figure 2b and those for C_{10}OH, C_{11}OH, C_{12}OH, and C_{14}OH in Figure 2c.

The phase diagrams for all of the binary mixtures investigated are rather asymmetric and have a UCST. The binodals are steep at small concentrations of the salt and become flat at higher concentrations. The critical composition, which in binary mixtures agrees with the maximum temperature of the phase diagrams, is located at low concentrations, in the mole fraction range $0.1 < x_{IL} < 0.2$.

The UCST increases with the chain length of the alcohol. This is a general observation that is expected on the basis of polarity considerations and in agreement with observations for other solutions of ILs.[1,2,71−75] Reducing the polarity of the solvent by using a larger chain length of the alcohol reduces the stability of the ionic solution, thereby increasing the separation temperature. Analogously, increasing the length of the side chain of the cation enhances the hydrophobicity of the IL and thus the solubility in weakly polar organic solvents, which corresponds to a decrease in the separation temperature. These trends are well-known and have been found for solutions of ILs with BF_4^- or PF_6^- as the anion.[54−62] Thus, phase separation with a UCST near ambient temperature was observable for solutions of C_{12}mimNTf$_2$ in *n*-alkyl alcohols with $n = 10$ to 20,[2] for solutions of C_8mimNTf$_2$ and C_{10}mimNTf$_2$ in *n*-alkyl alcohols with $n = 8$ to 20,[1] and for solutions of C_6mimNTf$_2$ in *n*-alkyl alcohols with $n = 6$ to 14. Measurements on solutions with larger or smaller alcohol chain lengths were outside the temperature range accessible with the present equipment.

The curves drawn in Figure 2a−c are fits based on eq 4 (solid lines) and eq 5 (dashed lines), which will be introduced and explained in the next section. The difference in the fits is not noticeable on the scale of Figure 2a. Although the difference

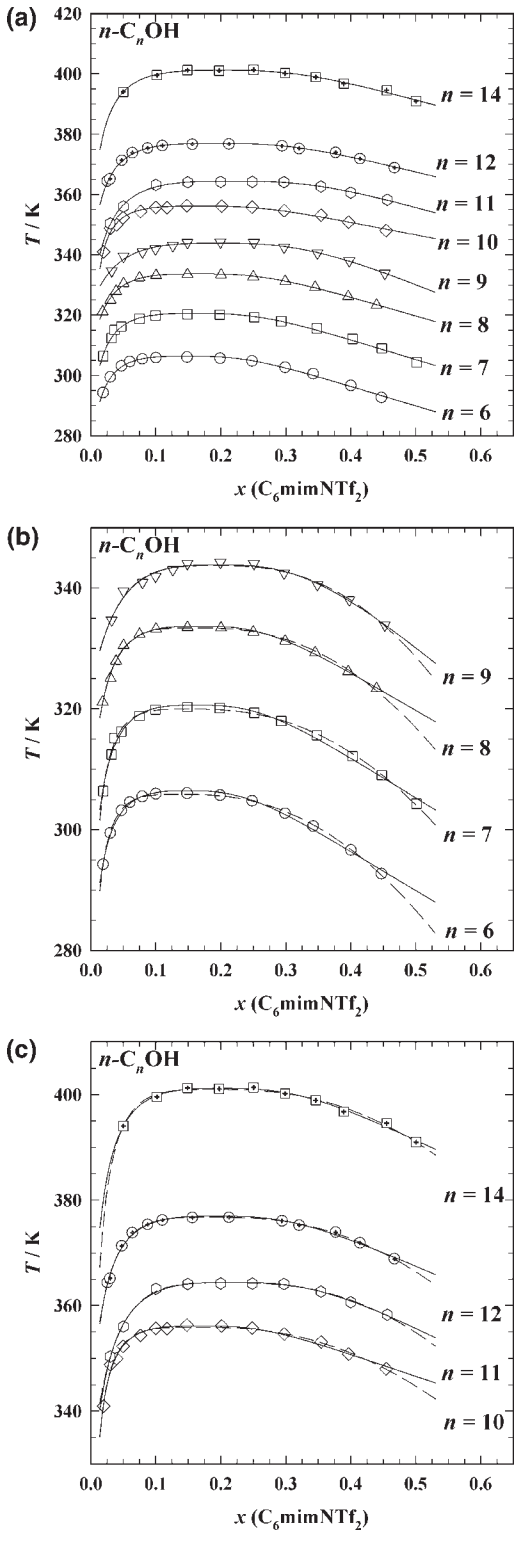

Figure 2. Isobaric phase diagrams [temperature (T) vs IL mole fraction (x)] at ambient pressure for C_6mimNTf$_2$ mixtures with n-alkyl alcohols (C_nOH). (a) Overview: ○, n = 6; □, n = 7; △, n = 8; ▽, n = 9; ◇, n = 10; ⬡, n = 11; ○ with cross, n = 12; □ with cross, n = 14. (b) Expanded view for n = 6, 7, 8, 9. (c) Expanded view for n = 10, 11, 12, 14. The uncertainties in T and x are not visible in the resolution of the plot. The curves were obtained by fitting the experimental data with eq 4 (solid lines) and eq 5 (dashed lines). The values of the fitting parameters are shown in Table 2.

between the two fits appears not to be important for the region investigated, it would be expected to become relevant at higher concentrations of the salt. Therefore, we have shown the fits also at mole fractions higher than those considered in the present experiment. A detailed discussion of the phase diagrams required a numerical analysis, as the maxima were difficult to determine because the tops of the curves were very flat and the shape of the curves appeared rather similar for all of the systems. In the following section, we will discuss the results of the fits, which provide a quantitative assessment of the critical data and the parameters describing the shape of the phase diagrams.

Shape Analysis of the Coexistence Curves. In order to allow for a quantitative assessment, the phase diagrams were analyzed by fitting the data in order to yield the parameters characterizing the curves. The steps that led to the working equations have been explained in detail in former work.[2,69] Therefore, we give here only the working equations with a short explanation of the background. The expressions applied are based on the scaling laws used in the field of critical phenomena.[4,14−16,50,51] For liquid−liquid phase transitions of binary solutions, the so-called Wegner expansion describes the temperature dependence of the mole fractions x_+ and x_- in the two phases and that of the so-called diameter $x_m = (x_+ + x_-)/2$ as power series in $T_c - T$, where T_c is the UCST. We neglected some contributions that were expected to be small because of the rather small temperature range of (10 to 15) K in the vicinity of the critical point investigated in this work. We treated the linear term and the term with the exponent $1 - \alpha$ that contributes to the temperature dependence of the diameter as a single linear term, because those two terms could hardly be separated in the fitting procedure. The resulting simplified scaling laws are

$$x_\pm - x_m = \pm B\cdot(T_c - T)^\beta \qquad (1)$$

where

$$x_m = x_c + A\cdot(T_c - T) + C\cdot(T_c - T)^{2\beta} \qquad (2)$$

We approximated the critical exponent β as $\beta = {}^1/_3$, as was done by Guggenheim.[83] This value is near the Ising value β = 0.326[4,14,16] but more convenient for the numerical analysis. Expanding $|x - x_m|^3$ to first order in A and C, solving for T, and expressing $T_c - T$ in the formula for x_m using the asymptotic power law yields T as a function of x:

$$T = T_c - \frac{|x - x_c|^3}{B^3 \pm 3A\cdot|x - x_c|^2 \pm 3\cdot C\cdot B|x - x_c|} \qquad (3)$$

The positive and negative signs correspond to the ranges $x < x_c$ and $x > x_c$, respectively. Thus, Ising criticality and the asymmetry of the phase diagrams are taken into account in a manner suitable for a fitting procedure. However, it turned out that the data for most of the phase diagrams analyzed in this paper did not allow for an unambiguous determination of both of the parameters A and C in eq 3. In some cases, no stable fit could be obtained. In other cases, the asymptotic standard errors (ASEs) of the parameters A and C came out as large as or even larger than the parameters themselves.

Therefore, we applied two simplified versions of eq 3. One presumed a linear temperature dependence of the diameter in eq 2 that was determined by the coefficient A, yielding the expression

$$T = T_c - \frac{|x - x_c|^3}{B^3 \pm 3A\cdot|x - x_c|^2} \qquad (4)$$

Table 2. Parameters for the Liquid−Liquid Phase Diagrams of Solutions of the Ionic Liquid C_6mimNTf_2 in *n*-Alkyl Alcohols As Obtained by Fitting the Experimental Curves with Equations 4 and 5 Using the Mole Fraction as the Composition Variable: Upper Critical Solution Temperatures (T_c), Critical Mole Fractions (x_c), Widths of the Coexistence Curves (B), and Values of the Parameters A and C That Determine the Rectilinear Diameter, Along with Their Asymptotic Standard Errors Provided by the Fitting Routine; Standard Deviation of the Residuals (σ); Coefficients (B^* and C^*) and Standard Deviations of the Residuals (σ^*) Obtained by Fitting the Phase Diagrams Represented Using Corresponding-State Variables

		T_c		B	A	C	σ			
solvent	fit eq	K	x_c	$K^{-1/3}$	K^{-1}	$K^{-2/3}$	K	B^*	C^*	$10^4 \cdot \sigma^*$
C_4OH[a]	4	269.42 ± 0.07	0.120 ± 0.002	0.069 ± 0.001	0.0068 ± 0.0007	–	0.17	3.69 ± 0.03	15.17 ± 0.66	6.49
	5	269.25 ± 0.06	0.114 ± 0.001	0.076 ± 0.001	–	0.0160 ± 0.0005	0.16	4.33 ± 0.03	5.85 ± 0.20	5.78
C_5OH[a]	4	289.84 ± 0.15	0.135 ± 0.003	0.073 ± 0.001	0.0061 ± 0.0009	–	0.44	3.59 ± 0.04	13.09 ± 0.55	15.37
	5	289.38 ± 0.07	0.127 ± 0.001	0.086 ± 0.000	–	0.0180 ± 0.0004	0.22	4.47 ± 0.02	6.22 ± 0.11	7.76
C_6OH[b]	4	306.32 ± 0.21	0.146 ± 0.005	0.078 ± 0.002	0.0062 ± 0.0015	–	0.34	3.58 ± 0.07	12.99 ± 1.13	11.29
	5	306.04 ± 0.07	0.136 ± 0.002	0.087 ± 0.000	–	0.0171 ± 0.0004	0.12	4.30 ± 0.02	5.73 ± 0.16	3.86
C_6OH[a]	4	306.81 ± 0.23	0.157 ± 0.004	0.078 ± 0.001	0.0047 ± 0.0013	–	0.69	3.35 ± 0.05	9.21 ± 0.41	22.74
	5	305.89 ± 0.16	0.140 ± 0.003	0.092 ± 0.001	–	0.0188 ± 0.0006	0.52	4.44 ± 0.03	6.11 ± 0.20	16.81
C_6OH	4	306.39 ± 0.17	0.149 ± 0.003	0.078 ± 0.001	0.0058 ± 0.0012	–	0.36	3.54 ± 0.05	11.93 ± 0.64	11.89
	5	305.87 ± 0.07	0.136 ± 0.002	0.089 ± 0.001	–	0.0183 ± 0.0004	0.15	4.42 ± 0.02	6.09 ± 0.14	5.07
C_7OH	4	320.60 ± 0.25	0.162 ± 0.004	0.083 ± 0.002	0.0057 ± 0.0016	–	0.56	3.49 ± 0.07	11.36 ± 0.71	16.97
	5	319.95 ± 0.16	0.148 ± 0.003	0.095 ± 0.001	–	0.0189 ± 0.0007	0.38	4.38 ± 0.03	5.96 ± 0.24	11.25
C_8OH[a]	4	334.15 ± 0.64	0.197 ± 0.009	0.089 ± 0.004	0.0032 ± 0.0036	–	1.75	3.14 ± 0.13	5.36 ± 0.45	52.40
	5	333.36 ± 0.16	0.154 ± 0.003	0.097 ± 0.001	–	0.0188 ± 0.0006	0.50	4.38 ± 0.03	5.86 ± 0.18	15.13
C_8OH[c]	4	332.03 ± 0.21	0.163 ± 0.006	0.080 ± 0.002	0.0065 ± 0.0020	–	0.49	3.38 ± 0.09	13.21 ± 1.61	14.83
	5	331.78 ± 0.17	0.150 ± 0.005	0.087 ± 0.001	–	0.0181 ± 0.0012	0.41	4.04 ± 0.06	5.81 ± 0.51	12.21
C_8OH	4	333.69 ± 0.16	0.166 ± 0.003	0.087 ± 0.001	0.0060 ± 0.0004	–	0.32	3.62 ± 0.04	12.06 ± 0.74	9.49
	5	333.40 ± 0.16	0.158 ± 0.003	0.095 ± 0.001	–	0.0161 ± 0.0009	0.33	4.18 ± 0.05	4.90 ± 0.29	9.92
C_9OH	4	343.83 ± 0.23	0.196 ± 0.007	0.095 ± 0.002	0.0043 ± 0.0020	–	0.50	3.38 ± 0.07	7.53 ± 1.44	14.26
	5	343.70 ± 0.25	0.188 ± 0.009	0.099 ± 0.002	–	0.0114 ± 0.0018	0.54	3.68 ± 0.07	2.98 ± 0.66	15.65
$C_{10}OH$	4	356.17 ± 0.22	0.169 ± 0.004	0.094 ± 0.002	0.0091 ± 0.0021	–	0.53	3.95 ± 0.09	19.16 ± 1.65	13.41
	5	355.92 ± 0.21	0.160 ± 0.004	0.105 ± 0.002	–	0.0221 ± 0.0021	0.52	4.67 ± 0.09	6.95 ± 0.45	12.99
$C_{11}OH$	4	364.41 ± 0.22	0.217 ± 0.004	0.104 ± 0.002	0.0062 ± 0.0021	–	0.31	3.40 ± 0.06	10.32 ± 1.23	8.62
	5	364.34 ± 0.16	0.207 ± 0.004	0.108 ± 0.002	–	0.0150 ± 0.0019	0.29	3.72 ± 0.06	3.69 ± 0.34	7.93
$C_{12}OH$	4	376.96 ± 0.20	0.194 ± 0.004	0.100 ± 0.002	0.0072 ± 0.0017	–	0.39	3.72 ± 0.06	13.99 ± 1.36	10.29
	5	376.75 ± 0.16	0.184 ± 0.004	0.107 ± 0.002	–	0.0180 ± 0.0015	0.32	4.21 ± 0.06	5.10 ± 0.35	8.58
$C_{14}OH$	4	401.16 ± 0.20	0.202 ± 0.006	0.098 ± 0.002	0.0065 ± 0.0025	–	0.35	3.58 ± 0.09	12.99 ± 1.49	8.82
	5	400.96 ± 0.22	0.187 ± 0.012	0.106 ± 0.002	–	0.0189 ± 0.0018	0.41	4.18 ± 0.07	5.49 ± 1.04	10.36

[a] Data from ref 75. [b] Data from ref 62. [c] Data from ref 76.

The other included the 2β term with the coefficient C as the only term determining the asymmetry of the phase diagram, leading to the equation

$$T = T_c - \frac{|x - x_c|^3}{B^3 \pm 3 \cdot C \cdot B|x - x_c|} \quad (5)$$

The results of the fits using these two simplified equations are given in Table 2 together with the ASEs provided by the fitting routine for all of the quantities as well as the standard deviations of the fit residuals (σ). The residuals of the fits with eqs 4 and 5 are shown in Figure 3a,b, respectively. At small concentrations, where the phase diagrams are steep and thus the uncertainties in the measured temperatures are large, the scatter of the data is outside the standard deviation. From a visual comparison of the residuals, the difference in the two fits appears to be marginal. However, the mean square deviations of the fits for the different systems (shown in Table 2) are systematically smaller for the fits with eq 5. Although the number of parameters is identical, the overall standard deviation for the fits with eq 4 for all of the systems was σ = 0.42 K, which is greater than the corresponding σ value of 0.37 K for the fits based on eq 5.

We now discuss how the parameters T_c, x_c, B, A, and C obtained from the fits vary with the chain length of the *n*-alkyl alcohol. Table 2 shows that with the exception of the critical temperature T_c, all of the other variables, namely, the critical mole fraction x_c, the width parameter B, and the parameters A and C determining the diameter, do not vary much with the chain length of the alcohol.

At first we discuss the results obtained for the critical-point data of the solutions of C_6mimNTf_2. Figure 4a shows the critical temperature T_c as function of the chain length of the alcohol. The figure includes results for solutions in butan-1-ol, pentan-1-ol, hexan-1-ol, and octan-1-ol obtained from the analysis of the data reported by other groups.[62,75,76] The agreement with the data reported by other groups for solutions in C_6OH[62,75,76] and C_8OH[75,76] is perfect. The solid symbols are the results obtained using the data reported in this work, while the open symbols are based on data reported by others. The squares are the results

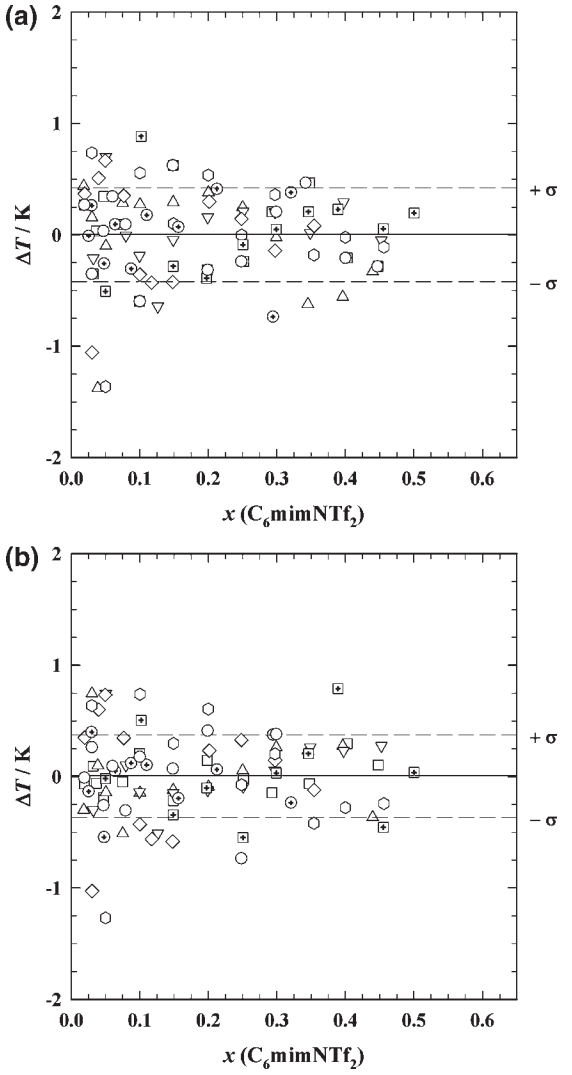

Figure 3. Deviations of the fitting results ($\Delta T = T_{fit} - T_{exptl}$) for the investigated systems using (a) eq 4 and (b) eq 5. The overall standard deviations (σ) are marked; the symbols denote the same *n*-alkyl alcohols (C_nOH) as in Figure 2: ○, $n = 6$; □, $n = 7$; △, $n = 8$; ▽, $n = 9$; ◇, $n = 10$; ⬡, $n = 11$; ○ with cross, $n = 12$; □ with cross, $n = 14$.

obtained by fitting with eq 4, and the circles represent the results obtained by fitting with eq 5. The symbols are kept the same for the other panels of Figure 4 showing results for the other parameters.

The estimates of the critical temperature obtained from the fits with eqs 4 and 5 are very similar and cannot be distinguished on the temperature scale of Figure 4a. The ASE figures are too small to be seen on the scale of this plot. Comparing the data from the numerical analysis (Table 2), we see that the analysis using eq 4 yields somewhat higher figures; the differences, however, are essentially within the ASE estimated for the fit.

The relation between the chain length of the solvent and the UCST is almost linear but has a minute S-shaped bend. This observation corroborates the observation of a bend to higher temperatures for large alcohol chain lengths in solutions of C_8mimNTf$_2$ and C_{10}mimNTf$_2$,[1] while for solutions of C_{12}mimNTf$_2$,[2] a bend to lower temperatures was observed. Similar behavior was observed for alcohol solutions of $C_x$mimBF$_4$ and $C_x$mimPF$_6$.[55]

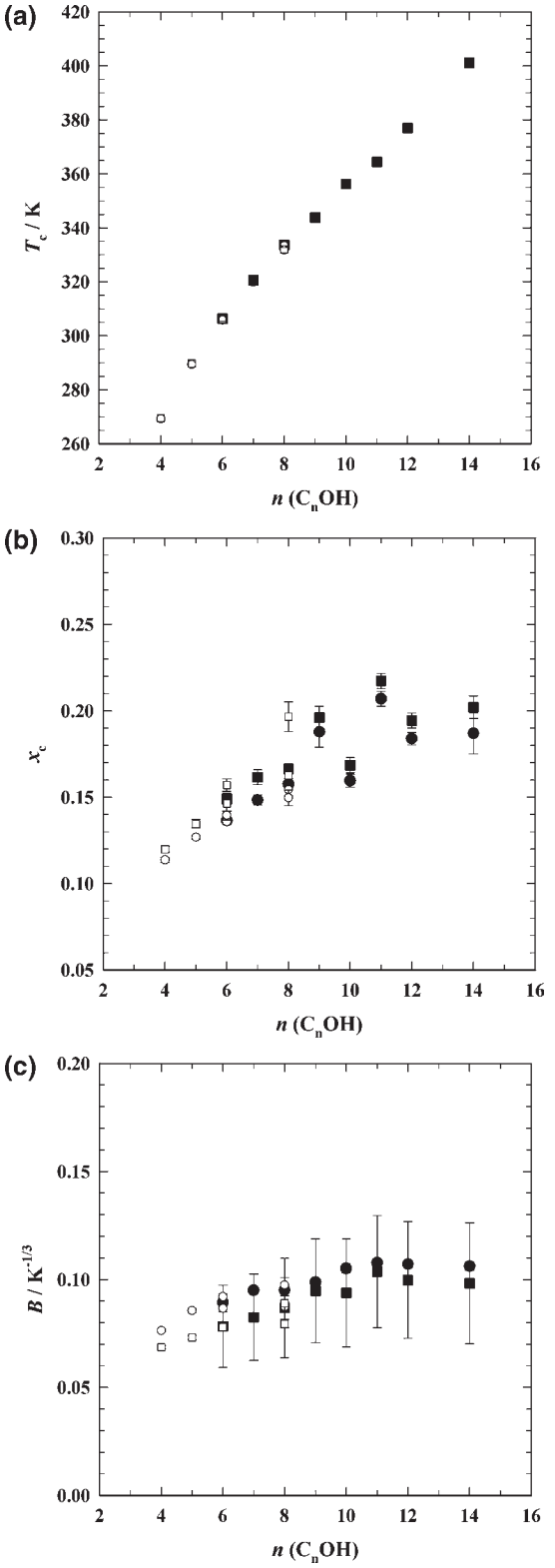

Figure 4. Representations of the characteristics of the phase diagrams for C_6mimNTf$_2$ + *n*-alkyl alcohol mixtures as result of fitting with eqs 4 (□) and 5 (○) as functions of the chain length *n* of the *n*-alkyl alcohol C_nOH: (a) critical temperature (T_c); (b) critical mole fraction (x_c); (c) width of the coexistence region (B). The uncertainties in T_c and the differences between the results for the two fitting methods are not visible in the resolution of the plot. Results from the present study are marked with solid symbols and data from the literature[62,75,76] with open symbols.

Figure 4b shows the critical mole fraction x_c as a function of the chain length of the alcohol. As for the critical temperature, we have included results obtained by evaluating the data reported by other groups. The value of the critical composition increases with the chain length of the alcohol, leveling off at large chain lengths. It seems, however, that the increase is stronger when the chain length of the alcohol is an odd number, so x_c appears to oscillate. The analysis of the phase diagrams of the ILs C_8mimNTf$_2$,[1] C_{10}mimNTf$_2$,[1] and C_{12}mim NTf$_2$[2] in *n*-alkyl alcohols also yielded an increase with the chain length of the alcohols, with indications of a similar modulation. The results for the critical composition as obtained by the different fit methods are noticeably different: the fits assuming the validity of the rectilinear diameter rule yield figures for the critical composition that are always about 0.01 higher than those obtained from the fits taking only the 2β term into account. The bend in the nonlinear diameter in eq 5 leads to a smaller figure for the estimate of the critical mole fraction than the fit based on eq 4. This deviation is larger than the ASE value obtained for the fits. In a preceding publication,[2] a comparison between the estimates of the critical composition x_c with the figure obtained by determining the critical mole fraction experimentally applying the equal volume criteria showed that the figure obtained with eq 5 is in better agreement with the experimental value than that obtained using eq 4.

We now turn to a discussion of the parameters describing the shape of the phase diagrams. Figure 4c shows the values of the width *B* obtained from the fits with the two methods. The widths obtained using eq 4 are larger than those from eq 5. The observable trends are similar to those found for x_c . We see an increase with the chain length of the alcohol, with indications of a maximum for $n = 11$ and a minute modulation between the values for even and odd numbers of carbon atoms in the alcohol chain, although this modulation is smaller than the ASE value of the fits.

While the T_c, x_c, and *B* values vary systematically with the chain length of the alcohol, the parameters *A* and *C* obtained using eqs 4 and 5, respectively, show no clear trend. The data appear to be randomly scattered. The particularly large ASE value for the fits with eq 4 is noteworthy and may be taken as a further indication that the phase diagrams are better described by eq 5, which approximates the diameter by the 2β term, than by eq 4, which is based on the rectilinear diameter rule.

Corresponding-States Analysis of the Phase Diagrams. In view of the large number of new systems, it is appropriate to search for a comprehensive overview. A powerful tool for reducing data and pinpointing general aspects of the systems under consideration is the concept of corresponding states,[83] which goes back to van der Waals.[11] Guggenheim's analysis of the phase diagrams of the liquid−gas phase transitions of the noble gases[83] demonstrated not only the approximate validity of the corresponding-states approach for this group of compounds but also showed that the coexistence curves are in accordance with the Ising model but not with any mean-field theory. Corresponding-states analysis allows the selection of certain groups for which the corresponding-states principle is satisfied, as was demonstrated, for example, by analyzing surface tensions[84,85] and phase diagrams.[86,87]

The theorem of corresponding states implies that scaling the thermodynamic variables by their critical values leads to a universal representation of the thermodynamic properties (e.g., of the phase diagrams). The phase diagrams match on a master curve when represented in terms of variables that are scaled in such a manner. This was observed also for solutions of ionic liquids.[30,55,63,66,69,86,87]

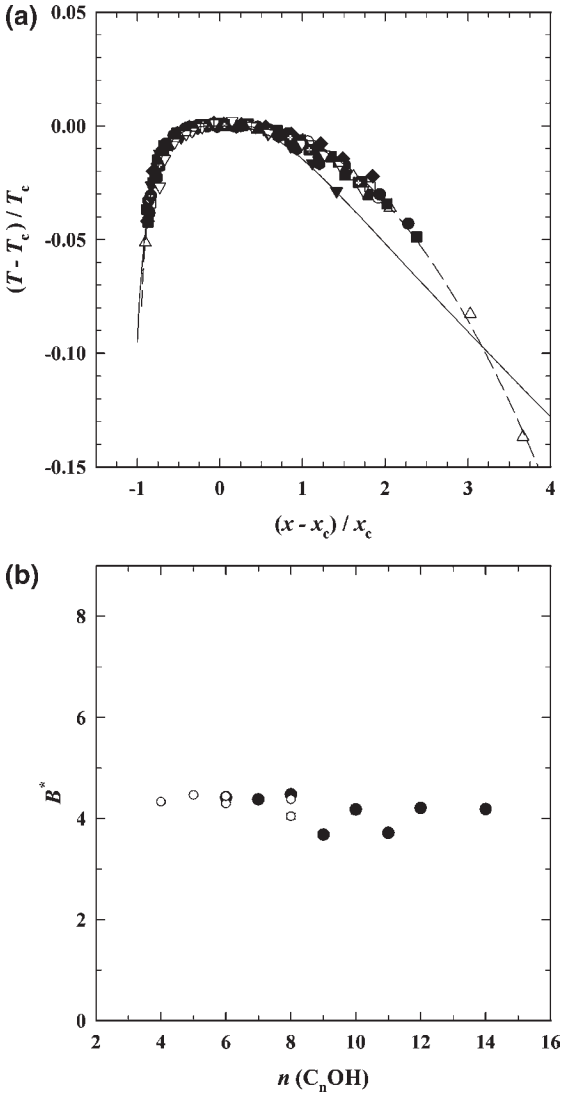

Figure 5. (a) Master plot of the phase diagrams of the solutions of C_6mimNTf$_2$ in *n*-alkyl alcohols and fits to the reduced data for C_6mimNTf$_2$ + octan-1-ol (△).[75] The fits were obtained using eq 4 (solid line) and eq 5 (dashed line). Symbols denote the same *n*-alkyl alcohols (C_nOH) as in Figure 2: ○, $n = 6$; □, $n = 7$; △, $n = 8$; ▽, $n = 9$; ◇, $n = 10$; ⬡, $n = 11$; ○ with cross, $n = 12$; □ with cross, $n = 14$. (b) Width of the coexistence region of the phase diagram (B^*) as obtained using eq 5. In both panels, the results of the present study are marked with solid symbols and data from the the literature[62,75,76] with open symbols.

Figure 5a shows the master plot of the phase diagrams of the solutions of C_6mimNTf$_2$ in alcohols based on critical data taken from fits using eq 5. The reduced temperature is $|T - T_c|/T_c$ and the reduced the mole fraction is $(x - x_c)/x_c$. The very reasonable representation of the phase diagrams of the solutions of C_6mimNTf$_2$ in alcohols is remarkable because of the rather large changes in the molecular shape and dielectric permittivity of the solvent. We mention that the analogous plot based on the critical data obtained from eq 4 leads to a less satisfactory representation with a larger scatter of the data points. The figure also shows the fits to the reduced data for C_6mimNTf$_2$ + octan-1-ol from ref 75, which cover a wider temperature range than our data. The fits were obtained using eq 4 (solid line) and eq 5 (dashed line) with the critical point fixed at the origin. It is obvious that eq 5, which

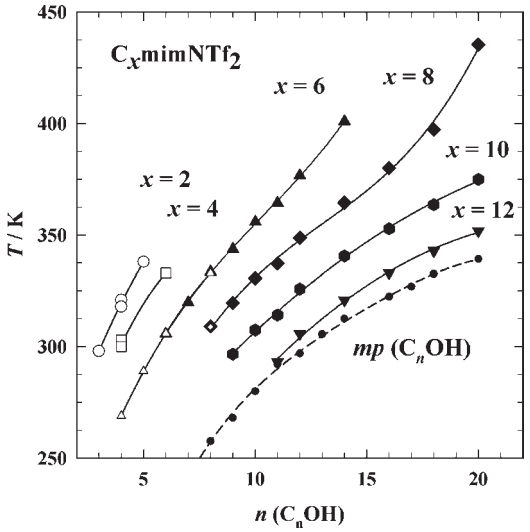

Figure 6. Dependence of the UCST on the chain length n of C_nOH for different $C_x$mimNTf$_2$: ○, $x = 2$; □, $x = 4$; △, $x = 6$ (this work); ◇, $x = 8$; ⬡, $x = 10$; ▽, $x = 12$. Data from this and previous work[1,2] are marked with solid symbols and data from the literature[61,62,74,75] with open symbols. The melting temperatures of the alcohols[88] are also shown to illustrate the principal chain-length dependence of the UCSTs of the investigated systems. Lines in the picture are given to illustrate trends and guide the eye.

describes the diameter by the 2β term, allows for a much better representation of the data than eq 4, which presumes a linear temperature dependence of the diameter.

Figure 5b shows that the width parameter B^* in the corresponding-states representation becomes constant, leading to the conclusion that the width B of the phase diagrams is a linear function of the critical mole fraction x_c. For the parameter C^* determining the diameter, no systematic trend can be identified.

General Discussion. In this work, we have reported phase diagrams of binary solutions of the IL C$_6$mimNTf$_2$ in the n-alkyl alcohols C_nOH with $6 < n < 14$ obtained by the synthetic method. The phase diagrams are accurate enough to allow for fitting with an approximate scaling relation that presumes Ising critical behavior and takes the asymmetry of the phase diagrams into account. The phase diagrams are described by a minimum set of four parameters, namely, the upper critical solution temperature (T_c) , the critical mole fraction (x_c), the width (B), and one parameter $(A$ or $C)$ for the diameter. As noticed in former work,[2,69] the assumption of a nonlinear temperature dependence determined by $(T_c - T)^{2\beta}$ with $\beta = {}^1/_3$ led to an improved representation of the data in comparison with the assumption of a linear temperature dependence.

As a result of the analysis, we found that the UCST increases almost linearly with the chain length of the solvent. The minute S-shaped bend was also observed for solutions of C$_8$mimNTf$_2$ and C$_{10}$mimNTf$_2$.[1] Data from other work were included into the analysis and found to fit nicely into this correlation. In comparison with the critical temperature, all of the other parameters describing the phase diagrams vary little for the different alcohol solutions. The numerical analysis showed that the critical mole fraction and the width increase with the chain length of the alcohol and appear to pass a shallow local maximum in the region of the alcohol chain length around $n = 11$. Indications of differences between alcohols with even and odd numbers of carbon atoms need to be substantiated. Again, the parameters obtained by analyzing the data of others were in agreement with this correlation. The fits that presume the temperature variation of the diameter with the exponent 2β led to lower values of the critical mole fraction than those obtained from the fits that presume the rectilinear diameter rule. The lower value was found to be in better agreement with the experimental one.[2] The phase diagrams of the solutions of C$_6$mimNTf$_2$ in alcohols in terms of the reduced variables $|T - T_c|/T_c$ and $(x - x_c)/x_c$ became almost identical, which is remarkable because of the rather large changes in the molecular shape and dielectric permittivity of the solvent. Again, the corresponding-states diagram included the data of other researchers. The width of the phase diagrams was the same for all systems. The description of the diameter by the 2β term yields a much better representation of the data for C$_6$mimNTf$_2$ + octan-1-ol obtained by Lachwa et al.,[75] which cover a wider temperature range than our data, than the fit based on the assumption of a linear temperature dependence. Thus, use of the theoretically based critical exponents of the phase diagram is advantageous even for data obtained by the cloud-point method, which are limited in their precision.

In order to put our results in the context of other work where phase diagrams with shorter and longer side chains of $C_x$mimNTf$_2$ were investigated, we show in Figure 6 the critical temperatures determined for our systems together with those from the literature[61,62,74−76] and the former reports.[1,2]

Figure 6 shows a systematic increase in the UCST with increasing chain length of the alcohol, with the slope decreasing as the length of the side chain increases. The increase in the critical temperatures of the alcohol mixtures with C$_{12}$mimNTf$_2$, however, becomes smaller with increasing chain length of the alcohols; this is different from the behavior found for $C_x$mimNTf$_2$ solutions with $x < 10$, where the increase in the critical temperatures is enhanced. The new measurements on the C$_6$mimNTf$_2$ solutions corroborate this observation.

The figure also includes the melting temperatures of the pure alcohols.[88] The curves describing how the critical temperatures of the solutions of the ILs with long side chains depend on the chain length of the alcohol are remarkably similar to the curve showing the melting temperatures of the alcohols.

Further elucidation of the critical data and the shape of the phase diagrams by correlation with other properties, such as the dielectric permittivity, the density, and the molecular structure, is beyond the scope of this work and will be given elsewhere.

AUTHOR INFORMATION

Corresponding Author

*Tel.: +49 421 218 3334. Fax: +49 421 218 7555. E-mail: rathke@uni-bremen.de.

ACKNOWLEDGMENT

We thank the colleagues in the Priority Program SPP-1191 for discussions and shared insight. This work was supported by the German Research Foundation (DFG) within the Priority Program SPP-1191 "Ionic Liquids" (Grants RA 1054/2-1 and SCHR 188/10-1).

REFERENCES

(1) Vale, V. R.; Rathke, B.; Will, S.; Schröer, W. Liquid−Liquid Phase Behavior of Solutions of 1-Octyl- and 1-Decyl-3-methylimidazolium Bis-(trifluoromethylsulfonyl)imide (C$_{8,10}$mimNTf$_2$) in n-Alkyl Alcohols. *J. Chem. Eng. Data* **2010**, *55*, 2030–2038.

(2) Vale, V. R.; Rathke, B.; Will, S.; Schröer, W. Liquid−Liquid Phase Behavior of Solutions of 1-Dodecyl-3-methylimidazolium Bis(-(trifluoromethyl)sulfonyl)amide (C_{12}mimNTf$_2$) in *n*-Alkyl Alcohols. *J. Chem. Eng. Data* **2010**, *55*, 4195–4205.

(3) Prausnitz, J. M.; Lichtenthaler, R. N.; de Azevedo, E. G. *Molecular Thermodynamics of Fluid Phase Equilibria*, 2nd ed.; Prentice-Hall: Englewood Cliffs, NJ, 1986.

(4) Rowlinson, J. S.; Swinton, F. L. *Liquids and Liquid Mixtures*, 3rd ed.; Butterworths: London, 1982.

(5) (a) Reid, R. C.; Prausnitz, J. M.; Sherwood, T. K. *The Properties of Gases and Liquids*, 3rd ed.; McGraw Hill: New York, 1977. (b) Poling, B. E.; Prausnitz, J. M.; O'Connell, J. P. *The Properties of Gases and Liquids*, 5th ed.; McGraw Hill: New York, 2001.

(6) Zhao, H. Innovative Applications of Ionic Liquids as "Green" Engineering Liquids. *Chem. Eng. Commun.* **2006**, *193*, 1660–1677.

(7) Plechkova, N. V.; Seddon, K. R. Applications of ionic liquids in the chemical industry. *Chem. Soc. Rev.* **2008**, *37*, 123–150.

(8) *Ionic Liquids: Industrial Applications for Green Chemistry*; Rogers, R. D., Seddon, K. R., Eds.; ACS Symposium Series 818; American Chemical Society: Washington, DC, 2002.

(9) *Ionic Liquids as Green Solvents: Progress and Prospects*; Rogers, R. D., Seddon, K. R., Eds.; ACS Symposium Series 856; American Chemical Society: Washington, DC, 2003.

(10) *Ionic Liquids in Synthesis*, 2nd ed.; Wasserscheid, P., Welton, T., Eds.; Wiley-VCH: Weinheim, Germany, 2008.

(11) Van der Waals, J. D. *On the Continuity of the Gaseous and Liquid States*; Rowlinson, J. S., Ed.; Studies in Statistical Mechanics, Vol. XIV; North-Holland: Amsterdam, 1988.

(12) Hildebrand, J. H.; Prausnitz, J. M.; Scott, R. L. *Regular and Related Solutions*; Van Nostrand Reinhold: New York, 1970.

(13) Guggenheim, E. A. *Mixtures*; Clarendon Press: Oxford, U.K., 1952.

(14) Domb, C. *The Critical Point*; Taylor and Francis: London, 1996.

(15) Anisimov, M. A. *Critical Phenomena in Liquids and Liquid Crystals*; Gordon and Breach: Philadelphia, 1991.

(16) Ivanov, D. Y. *Critical Behavior of Non-Ideal Systems*; Wiley-VCH: Weinheim, Germany, 2008.

(17) Kim, Y. C.; Anisimov, M. A.; Sengers, J. V.; Luijten, E. Crossover critical behavior in the three-dimensional Ising model. *J. Stat. Phys.* **2003**, *110*, 591–609.

(18) De Pablo, J. J.; Prausnitz, J. M. Thermodynamics of Liquid−Liquid Equilibria Including the Critical Region. *AIChE J.* **1988**, *34*, 1595–1606.

(19) Anisimov, M. A.; Povodyrev, A. A.; Sengers, J. V. Crossover critical phenomena in complex fluids. *Fluid Phase Equilib.* **1999**, *158*, 537–547.

(20) White, J. A. Are global renormalization methods capable of locating gas−liquid critical points?. *Int. J. Thermophys.* **2000**, *22*, 1147–1157.

(21) Hendriks, E.; Kontogeorgis, G. M.; Dohrn, R.; de Hemptinne, J. C.; Economou, I. G.; Zilnik, L. F.; Vesovic, V. Industrial Requirements for Thermodynamics and Transport Properties. *Ind. Eng. Chem. Res.* **2010**, *49*, 11131–11141.

(22) Kayser, R. F.; Raveche, H. J. Asymptotic density correlations and corrections to scaling for fluids with non-finite-range interactions. *Phys. Rev. A* **1984**, *29*, 1013–1015.

(23) Pitzer, K. S. Critical Phenomena in Ionic Fluids. *Acc. Chem. Res.* **1990**, *23*, 333–338.

(24) Fisher, M. E. The Story of Coulombic Criticality. *J. Stat. Phys.* **1994**, *75*, 1–36.

(25) Stell, G. Criticality and Phase-Transitions in Ionic Fluids. *J. Stat. Phys.* **1995**, *78*, 197–238.

(26) Weingärtner, H.; Schröer, W. Criticality of Ionic Fluids. *Adv. Chem. Phys.* **2001**, *116*, 1–66.

(27) Wiegand, S.; Briggs, M. E.; Levelt Sengers, J. M. H.; Kleemeier, M.; Schröer, W. Turbidity, light scattering, and coexistence curve data for the ionic binary mixture triethyl *n*-hexyl ammonium triethyl *n*-hexyl borate in diphenyl ether. *J. Chem. Phys.* **1998**, *109*, 9038–9051.

(28) Kleemeier, M.; Wiegand, S.; Schröer, W.; Weingärtner, H. The liquid−liquid phase transition in ionic solution: Coexistence curves of tetra-*n*-butylammonium picrate in alkylalcohols. *J. Chem. Phys.* **1999**, *110*, 3085–3099.

(29) Oleinikova, A.; Bonetti, M. Coexistence curve of the ionic binary mixture tetra-*n*-butylammonium picrate in 1-dodecanol. *Chem. Phys. Lett.* **1999**, *299*, 417–422.

(30) Wagner, M.; Stanga, O.; Schröer, W. The liquid−liquid coexistence of binary mixtures of the room temperature ionic liquid 1-methyl-3-hexylimidazolium tetrafluoroborate with alcohols. *Phys. Chem. Chem. Phys.* **2004**, *6*, 4421–4431.

(31) Schröer, W.; Wiegand, S.; Weingärtner, H. The effect of short-range hydrogen-bonded interactions on the nature of the critical point of ionic fluids. Part II: Static and dynamic light scattering on solutions of ethylammonium nitrate in *n*-octanol. *Ber. Bunsen-Ges. Phys. Chem.* **1993**, *97*, 975–982.

(32) Barthel, J.; Carl, E.; Gores, H. J. Coulombic liquid−liquid phase separation of dilithium hexafluoropropane-1,3-bis[sulfonylbis(trifluoromethylsulfonyl)methanide] solutions in diethyl carbonate. *Electrochem. Solid-State Lett.* **1999**, *2*, 218–221.

(33) Schröer, W.; Wagner, M.; Stanga, O. Apparent mean-field criticality of liquid−liquid phase transitions in ionic solutions. *J. Mol. Liq.* **2006**, *127*, 2–9.

(34) Caillol, J. M.; Levesque, D.; Weiss, J. J. Critical behavior of the restricted primitive model revisited. *J. Chem. Phys.* **2002**, *116*, 10794–10800.

(35) Orkoulas, G.; Panagiotopoulos, A. Z. Phase behavior of the restricted primitive model and square-well fluids from Monte Carlo simulations in the grand canonical ensemble. *J. Chem. Phys.* **1999**, *110*, 1581–1590.

(36) Yan, Q. L.; de Pablo, J. J. Hyper-parallel tempering Monte Carlo: Application to the Lennard-Jones fluid and the restricted primitive model. *J. Chem. Phys.* **1999**, *111*, 9509–9515.

(37) Leote de Carvalho, R. J. F.; Evans, R. Criticality of ionic fields—the Ginzburg criterion for the restricted primitive model. *J. Phys.: Condens. Matter* **1995**, *7*, L575–L583.

(38) Lee, B. P.; Fisher, M. E. Ginzburg criterion for Coulombic criticality. *Phys. Rev. Lett.* **1996**, *77*, 3561–3564.

(39) Schröer, W.; Weiss, V. C. Ginzburg criterion for the crossover behavior of model fluids. *J. Chem. Phys.* **1998**, *109*, 8504–8513.

(40) Singh, R. R.; Pitzer, K. S. Near-Critical Coexistence Curve and Critical Exponent of an Ionic Fluid. *J. Chem. Phys.* **1990**, *92*, 6775–6778.

(41) Zhang, K. C.; Briggs, M. E.; Gammon, R. W.; Levelt Sengers, J. M. H. The susceptibility critical exponent for a nonaqueous ionic binary mixture near a consolute point. *J. Chem. Phys.* **1992**, *97*, 8692–8697.

(42) Schröer, W. *Criticality of Ionic Liquids in Solution*; Henderson, D., Holovko, M., Trokhymchuk, A., Eds.; Ionic Matter: Modern Trends in Theory and Applications; NATO Science Series, Vol. 206; Springer: Dordrecht, 2005; pp 143−180.

(43) Levelt Sengers, J. M. H.; Harvey, A. H.; Wiegand, S. In *Equations of State for Fluids and Fluid Mixtures*; Sengers, J. V., Kayser, R. F., Peters, C. J., White, H. J., Eds.; Elsevier: Amsterdam, 2000; p 805.

(44) Kirshenbaum, A. D.; Cahill, J. A.; McGonigal, P. J.; Grosse, A. V. The density of liquid NaCl and KCl and an estimate of their critical constants together with those of other alkali halides. *J. Inorg. Nucl.Chem.* **1962**, *24*, 1287–1296.

(45) see ref 4, pp 72−73.

(46) Kim, Y. C.; Fisher, M. E.; Orkoulas, G. Asymmetric fluid criticality I. Scaling with pressure mixing. *Phys. Rev. E* **2003**, *67*, No. 061506.

(47) Cerdeiriña, C. A.; Anisimov, M. A.; Sengers, J. V. *Chem. Phys. Lett.* **2006**, *424*, 414–419.

(48) Wang, J.; Anisimov, M. A. Nature of vapor−liquid asymmetry in fluid criticality. *Phys. Rev. E* **2007**, *75*, No. 051107.

(49) Wang, J.; Cerdeiriña, C. A.; Anisimov, M. A.; Sengers, J. V. Principle of isomorphism and complete scaling for binary-fluid criticality. *Phys. Rev E.* **2008**, *77*, No. 031127.

(50) Ley-Koo, M.; Green, M. S. Consequences of the renormalization-group for the thermodynamics of fluids near the critical point. *Phys. Rev. A* **1981**, *23*, 2650–2659.

(51) Greer, S. C.; Das, B. K.; Kumar, A.; Gopal, E. S. R. Critical behavior of the diameters of liquid−liquid coexistence curves. *J. Chem. Phys.* **1983**, *79*, 4545–4552.

(52) Pérez-Sánchez, G.; Losada-Pérez, P.; Cerdeiriña, C. A.; Sengers, J. V.; Anisimov, M. A. Asymmetric criticality in weakly compressible liquid mixtures. *J. Chem. Phys.* **2010**, *132*, No. 154502.

(53) Behnejad, H.; Sengers, J. V.; Anisimov, M. A. Thermodynamic Behaviour of Fluids near Critical Points. In *Applied Thermodynamics of Fluids*; Goodwin, A. R. H., Sengers, J. V., Peters, C. J., Eds.; Royal Society of Chemistry: Cambridge, U.K., 2010; p 321−367.

(54) Anthony, J. L.; Maginn, E. J.; Brennecke, J. F. Solution Thermodynamics of Imidazolium-Based Ionic Liquids and Water. *J. Phys. Chem. B* **2001**, *105*, 10942–10949.

(55) Wagner, M.; Stanga, O.; Schröer, W. Corresponding states analysis of the critical points in binary solutions of room temperature ionic liquids. *Phys. Chem. Chem. Phys.* **2003**, *5*, 3943–3950.

(56) Cerdeiriña, C. A.; Troncoso, I.; Ramos, C. P.; Romani, L.; Najdanovic-Visak, V.; Guedes, H. J. R.; Esperança, J. M. S. S.; Visak, Z. P.; Nunes da Ponte, M.; Rebelo, L. P. N. Criticality of the $[C_4mim][BF_4]$ + water system. *ACS Symp. Ser.* **2005**, *901*, 175–186.

(57) Wu, C. T.; Marsh, K. N.; Deev, A. V.; Boxall, J. A. Liquid−liquid equilibria of room-temperature ionic liquids and butan-1-ol. *J. Chem. Eng. Data* **2003**, *48*, 486–491.

(58) Marsh, K. N.; Deev, A.; Wu, C. T.; Tran, E.; Klamt, A. K. Room temperature ionic liquids as replacements for conventional solvents—A review. *Korean J. Chem. Eng.* **2002**, *19*, 357–362.

(59) Sahandzhieva, K.; Tuma, D.; Breyer, S.; Kamps, A.; Maurer, G. Liquid−liquid equilibrium in mixtures of the ionic liquid 1-*n*-butyl-3-methylimidazolium hexafluorophosphate and an alkanol. *J. Chem. Eng. Data* **2006**, *51*, 1516–1525.

(60) Crosthwaite, J. M.; Muldoon, M. J.; Aki, S. V. N. K.; Maginn, E. J.; Brennecke, J. F. Liquid Phase Behavior of Ionic Liquids with Alcohols: Experimental Studies and Modeling. *J. Phys. Chem. B* **2006**, *110*, 9354–9361.

(61) Crosthwaite, J. M.; Aki, S. N. V. K.; Maginn, E. J.; Brennecke, J. F. Liquid phase behavior of imidazolium-based ionic liquids with alcohols. *J. Phys. Chem. B* **2006**, *108*, 5113–5119.

(62) Crosthwaite, J. M.; Aki, S. N. V. K.; Maginn, E. J.; Brennecke, J. F. Liquid phase behavior of imidazolium-based ionic liquids with alcohols: Effect of hydrogen bonding and non-polar interactions. *Fluid Phase Equilib.* **2005**, *228−229*, 303–309.

(63) Saracsan, D.; Rybarsch, C.; Schröer, W. *Z. Phys. Chem.* **2006**, *220*, 1417–1437.

(64) Domanska, U.; Casas, L. M. Solubility of phosphonium ionic liquid in alcohols, benzene, and alkylbenzenes. *J. Phys. Chem. B* **2007**, *111*, 4109–4115.

(65) Domanska, U.; Paduszynski, K. Phase equilibria study in binary systems (tetra-*n*-butylphosphonium tosylate ionic liquid + 1-alcohol, or benzene, or *n*-alkylbenzene). *J. Phys. Chem. B* **2008**, *112*, 11054–11059.

(66) Butka, A.; Vale, V. R.; Saracsan, D.; Rybarsch, C.; Weiss, V. C.; Schröer, W. The Liquid−Liquid Phase Transition in Solutions of Ionic Liquids with Halide Anions: Criticality and Corresponding States. *Pure Appl. Chem.* **2008**, *80*, 1613–1630.

(67) Lachwa, J.; Szydlowski, J.; Najdanovic-Visak, V.; Rebelo, L. P. N.; Seddon, K. R.; da Ponte, M. N.; Esperança, J. M. S. S.; Guedes, H. J. R. Evidence for Lower Critical Solution Behavior in Ionic Liquid Solutions. *J. Am. Chem. Soc.* **2005**, *127*, 6542–6543.

(68) Ferreira, R.; Blesic, M.; Trindade, J.; Marrucho, I.; Canongia-Lopes, J. N.; Rebelo, L. P. N. Solubility of fluorinated compounds in a range of ionic liquids. Cloud-point temperature dependence on composition and pressure. *Green Chem.* **2008**, *10*, 918–928.

(69) Schröer, W.; Vale, V. R. Liquid−liquid phase separation in solutions of ionic liquids: Phase diagrams, corresponding state analysis and comparison with simulations of the primitive model. *J. Phys.: Condens. Matter* **2009**, *21*, No. 424119.

(70) Shiflett, M. B.; Niehaus, A. M. S. Liquid−Liquid Equilibria in Binary Mixtures Containing Substituted Benzenes with Ionic Liquid 1-Ethyl-3-methylimidazolium Bis(trifluoromethylsulfonyl)imide. *J. Chem. Eng. Data* **2010**, *55*, 346–353.

(71) Lachwa, J.; Szydlowski, J.; Makowska, A.; Seddon, K. R.; Esperança, J. M. S. S.; Guedes, H. J. R.; Rebelo, L. P. N. Changing from an unusual high-temperature demixing to a UCST-type in mixtures of 1-alkyl-3-methylimidazolium bis{(trifluoromethyl)sulfonyl}amide and arenes. *Green Chem.* **2006**, *8*, 262–267.

(72) Heintz, A.; Lehmann, J.; Wertz, C.; Jacquemin, J. Thermodynamic properties of mixtures containing ionic liquids. 4. LLE of binary mixtures of $[C_2MIM][NTf_2]$ with propan-1-ol, butan-1-ol, and pentan-1-ol and $[C_4MIM][NTf_2]$ with cyclohexanol and 1,2-hexanediol including studies of the influence of small amounts of water. *J. Chem. Eng. Data* **2005**, *50*, 956–960.

(73) Wertz, Ch.; Tschersich, A.; Lehmann, J. K.; Heintz, A. Liquid−liquid equilibria and liquid−liquid interfacial tension measurements of mixtures containing ionic liquids. *J. Mol. Liq.* **2007**, *131−132*, 2–6.

(74) Heintz, A.; Lehmann, J.; Wertz, C. Thermodynamic properties of mixtures containing ionic liquids. 3. Liquid−liquid equilibria of binary mixtures of 1-ethyl-3-methylimidazolium bis(trifluoromethylsulfonyl)-imide with propan-1-ol, butan-1-ol, and pentan-1-ol. *J. Chem. Eng. Data* **2003**, *48*, 472–474.

(75) Lachwa, J.; Morgado, P.; Esperança, J. M. S. S.; Guedes, H. J. R.; Canongia Lopes, J. N.; Rebelo, L. P. N. Fluid-Phase Behavior of {1-Hexyl-3-methylimidazolium Bis(trifluoromethylsulfonyl) Imide, $[C_6mim][NTf_2]$, + C_2−C_8 *n*-Alcohol} Mixtures: Liquid−Liquid Equilibrium and Excess Volumes. *J. Chem. Eng. Data* **2006**, *51*, 2215–2221.

(76) Pereiro, A. B.; Deive, F. J.; Rodriguez, A.; Ruivo, D.; Lopes, J. N. C.; Esperança, J. M. S. S.; Rebelo, L. P. N. New Insight into Phase Equilibria Involving Imidazolium Bistriflamide Ionic Liquids and their Mixtures with Alcohols and Water. *J. Phys. Chem. B* **2010**, *114*, 8978–8985.

(77) Swatloski, R. P.; Holbrey, J. D.; Rogers, R. D. Ionic liquids are not always green: Hydrolysis of 1-butyl-3-methylimidazolium hexafluorophosphate. *Green Chem.* **2003**, *5*, 361–363.

(78) Costa Gomes, M. F.; Canongia Lopes, J. N.; Padua, A. A. H. Thermodynamics and Heterogeneity of Ionic Liquids. *Top. Curr. Chem.* **2009**, *290*, 161–183.

(79) Triolo, A.; Russina, O.; Bleif, H.; Cola, E. D. Nanoscale segregation in room temperature ionic liquids. *J. Phys. Chem. B* **2007**, *111*, 4641–4644.

(80) Bradley, A. E.; Hardacre, C.; Holbrey, J. D.; Johnston, S.; McMath, S. E. J.; Nieuwenhuyzen, M. Small-Angle X-ray Scattering Studies of Liquid Crystalline 1-Alkyl-3-methylimidazolium Salts. *Chem. Mater.* **2002**, *14*, 629–635.

(81) Holbrey, J. D.; Reichert, W. M.; Rogers, R. D. Crystal structures of imidazolium bis(trifluoromethanesulfonyl)imide 'ionic liquid' salts: The first organic salt with a *cis*-TFSI anion conformation. *Dalton Trans.* **2004**, 2267–2271.

(82) Wohlfarth, C. Static dielectric constants of pure liquids and binary liquid mixtures. *Landolt Börnstein, Numerical Data and Functional Relationships in Science and Technology*; Springer: Berlin, 1991; New Series IV/6.

(83) Guggenheim, E. A. The Principle of Corresponding States. *J. Chem. Phys.* **1945**, *13*, 253–261.

(84) Weiss, V. C.; Schröer, W. Anomalous corresponding-states surface tension of hydrogen fluoride and of the Onsager model. *J. Chem. Phys.* **2005**, *122*, No. 084705.

(85) Weiss, V. C.; Schröer, W. Corresponding-states analysis of the surface tension of simple, polar, and ionic fluids. *Int. J. Thermophys.* **2007**, *28*, 506–519.

(86) Schröer, W. Universality and Corresponding State Behaviour in the Phase Diagrams of Alcohol Solutions of Ionic Liquids with the BF_4^- Anion. *J. Mol. Liq.* **2006**, *125*, 164.

(87) Dittmar, H.; Butka, A.; Vale, V. R.; Schröer, W. Liquid−liquid phase transition in the ionic solutions of tetra-*n*-butylammonium chloride in *o*-xylene and ethylbenzene: Phase diagrams and corresponding state analysis. *J. Mol. Liq.* **2009**, *145*, 116.

(88) *Handbook of Chemistry and Physics*, 76th ed.; Lide, D. R., Ed.; CRC Press: Boca Raton, FL, 1995.